**e-ISSN:** 2687-6698

**Research Article**

Turkish Journal of

Analytical Chemistry

TurkJAC

https://dergipark.org.tr/tr/pub/turkjac

# Hydrometallurgy of lithium: Selective separation from geothermal brines using chitosan-lithium ion sieve composite*

**Yaşar Kemal Recepoğlu, Aslı Yüksel****

Izmir Institute of Technology, Department of Chemical Engineering, 35430, Urla, Izmir, Türkiye

## Abstract

This study investigates the selective recovery of lithium (Li) from geothermal brines using a chitosan-coated lithium manganese oxide composite (CTS/LMO). Geothermal brines from Germencik and Tuzla in Türkiye, characterized by distinct physicochemical properties, were used to evaluate adsorption performance. This study introduces a novel application of CTS/HMO adsorbent for selective lithium separation from real geothermal water samples from the Germencik and Tuzla regions, marking the first such investigation. The Freundlich isotherm provided the best fit for the adsorption data, indicating heterogeneous and multilayer adsorption, with maximum adsorption capacities of 3.622 mg/g for Germencik and 3.556 mg/g for Tuzla derived from the Langmuir isotherm. Kinetic studies revealed that lithium adsorption followed a pseudo-first-order model for Germencik ($R^2 = 0.992$) and a pseudo-second-order model for Tuzla ($R^2 = 0.914$). The intraparticle diffusion model identified boundary layer diffusion as a significant rate-limiting step, with diffusion rate constants of 0.365 mg/g·$h^{0.5}$ for Germencik and 0.588 mg/g·$h^{0.5}$ for Tuzla. Mechanistic studies demonstrated ion exchange as the dominant adsorption mechanism, supported by adsorption energy values of 8.64 kJ/mol for Germencik and 9.13 kJ/mol for Tuzla. Optimal conditions yielded lithium recovery efficiencies of 95% for Germencik and 80% for Tuzla, with the differences attributed to variations in salinity and ionic composition. CTS/LMO effectively retained Li up to 241 BV with 69.03% efficiency, while desorption peaked at 43 mg/L at 9 BV, achieving 76% elution efficiency in column operation with a model solution. These findings demonstrate the potential of CTS/LMO as an efficient and sustainable adsorbent for Li recovery from geothermal brines, contributing to the growing demand for Li in renewable energy applications.

**Keywords:** Adsorption, geothermal water, lithium, selective separation

## 1. Introduction

Lithium (Li) naturally occurs in various Earth environments, including igneous, volcanic, and sedimentary rocks, with concentrations ranging from 20 to 60 mg/kg [1]. It is also found in seawater at approximately 0.18 ppm, brines and salt marshes (sabkhas) at around 1000 ppm, and thermal fluids ranging from 15 to 350 ppm [2]. The high volatile content in late-stage magmatic fluids, combined with slow magma cooling, promotes the formation of Li-rich minerals in larger structures like pegmatites. These pegmatites often contain minerals such as phlogopite, tourmaline, spodumene ($LiAlSi_2O_6$), and zinwaldite (a Li-bearing mica found in certain granites). Globally, an estimated 31.1 million tons of Li are available from natural sources, with the largest reserves in brines (21.6 million tons), followed by pegmatites (3.9 million tons) [3,4]. Deposits of hectorite and jadarite account for about 3.4 million tons, while geothermal fluids contribute to 2 million tons [5]. Despite lower Li concentrations in geothermal waters than in brines, they still represent a significant source. Li concentrations in geothermal waters vary by region [6–9]. In Türkiye, sediments associated with thermal springs also have elevated Li concentrations [10–13]. The rising demand for electric vehicles has notably increased the need for Li, with about 8 kg required for a 60 kWh Li-ion battery. Global Li consumption, 280,000 tons in 2018, is expected to rise significantly to 1.2–1.6 million tons by 2030. Given the growing economic importance of Li, extracting valuable metals from geothermal fluids has become crucial for environmental and economic reasons [14–16].

**Citation:** Y.K. Recepoğlu, A. Yüksel, Hydrometallurgy of lithium: Selective separation from geothermal brines using chitosan-lithium ion sieve composite, Turk J Anal Chem, 7(2), 2025, 140–153.

****Author of correspondence:** asliyuksel@iyte.edu.tr
**Tel:** +90 (232) 750 66 09 **Fax:** +90 (232) 750 66 45

**Received:** January 30, 2024 **Accepted:** March 23, 2025
https://doi.org/10.51435/turkjac.1629713

---

**This paper was presented at the 6th International Environmental Chemistry Congress, EnviroChem 05-08 November 2024, Trabzon Türkiye.*

Extracting Li from brines remains one of the most cost-effective methods and has been utilized for a long time. Various techniques can be employed to recover Li from aqueous sources. Namely, the precipitation of Li as Li-aluminate has been documented, and the highest yield was achieved at room temperature [17]. Traditional liquid-liquid extraction methods, such as the beta-diketone/trioctylphosphine oxide process and more recent ionic liquid-based techniques, have also been employed [18]. Membrane technologies, such as electrodialysis with bipolar membranes and membrane electrolysis, have proven effective for Li recovery [19,20]. In addition, membranes containing (2-ethylhexyl)-diphenyl phosphate selectively separate Li+ ions from Mg2+ and Ca2+, while reverse osmosis and nanofiltration processes have shown 85% efficiency in separating Mg from Li in brines [21]. On the other hand, adsorption/ion exchange is emerging as a promising, environmentally friendly method for Li extraction from brines, geothermal water, and seawater, offering rapid recovery despite the need for large volumes of eluent and freshwater [22]. However, a major challenge in adsorption lies in the lack of suitable adsorbents for large-scale industrial applications, which limits its effectiveness in practical settings. As a mostly studied adsorbent type, Li-ion sieves (LISs) exhibit excellent Li screening capabilities due to their stable molecular framework, enabling efficient Li recovery from brines with high rates and selectivity [23]. LISs are classified into manganese-based (Mn-LIS) and titanium-based (Ti-LIS) types [24]. Mn-LISs are popular for their higher Li adsorption capacity, although they suffer from manganese loss, which may affect their cycling performance [25,26]. Xiao et al. synthesized a spinel-type Li4Mn5O12 through a solid-phase reaction, achieving a Li adsorption capacity of 39.62 mg/g at pH 10.1 using a LiCl-based model solution. Except for Mg2+, almost all competitor ions were fully rejected. After 55 adsorption-desorption cycles, the adsorption capacity remained at 2.78 mg/g [27]. In another study, Li1.6Mn1.6O4 was synthesized, resulting in a Li adsorption capacity of 42.1 mg/g at pH 10.1. After six cycles, the adsorption capacity decreased by 11.33%, from 28.36 mg/g to 25.15 mg/g, while maintaining high Li selectivity [28]. Zhang et al. synthesized LiMn2O4, which exhibited a Li adsorption capacity of 16.9 mg/g at pH 9.19, with high selectivity for Li+, followed by divalent ions ($Ca^{2+}$, $Mg^{2+}$), and then monovalent ions (K+, Na+) [29]. Moreover, spinel-type λ-MnO2 was used to recover Li from the Balçova geothermal water sample resourced from İzmir province, Türkiye, by adsorption and adsorption/ultrafiltration (UF) hybrid methods. The maximum Li sorption capacity was reported to be powdery and granulated λ-$MnO_2$ at 31.55 and 30.42 mg/g, respectively. Also, the adsorption-UF hybrid system efficiently handled fine particles, making it a favorable process for Li separation from geothermal water [30–32]. As LISs are in powder form, their practical use is limited due to poor fluidity, low permeability, and high energy consumption from pressure drops [22,23]. To overcome this, methods like foaming [33], fiber formation [34], and granulation [35,36] are employed, with granulation being the most promising nanoparticle modification. Granulated LISs offer high water permeability and mechanical and chemical stability. Chitosan, a hydrophilic and stable binder, improves adsorption capacity and reduces dissolution loss, making it widely used in the granulation of LMOs ($LiMn_2O_4$, $Li_4Mn_5O_{12}$, and $Li_{1.66}Mn_{1.66}O_4$) [37].

This study presents the application of chitosan-coated hydrometallurgically synthesized LMO (CTS/$LiMn_2O_4$) as an innovative adsorbent for Li extraction using geothermal brines from Germencik and Tuzla Geothermal Energy Power Plants located in the western Anatolia region of Türkiye coupling enhanced ease of operation due to the chitosan coating. This study also presents a novel approach by applying a previously developed CTS/HMO adsorbent to real geothermal water samples with varying characteristics from the Germencik (Aydın) and Tuzla (Çanakkale) regions for selective lithium separation—marking the first such application in the literature. While the experimental framework follows a classical approach, its implementation in actual geothermal brine systems yields significant and novel insights from an engineering perspective. The findings provide valuable implications for practical applications, particularly in advancing lithium recovery strategies. Furthermore, using a column method enhances the study's relevance for industrial-scale applications, reinforcing its potential for large-scale implementation.

## 2. Experimental

### 2.1. Materials

CTS/$LiMn_2O_4$ (CTS/LMO) adsorbent was synthesized, and the CTS/$HMn_2O_4$ (CTS/HMO) form of the adsorbent was prepared using the same method described in the literature [38]. A 1.0 mol/L manganese (II) nitrate ($Mn(NO_3)_2$) solution (100 mL) was prepared by dissolving 28.7 g of manganese (II) nitrate hexahydrate ($Mn(NO_3)_2{\cdot}6H_2O$) in deionized water, while 11.4 g of ammonium peroxodisulfide ($(NH_4)_2S_2O_8$) and 8.4 g of lithium hydroxide monohydrate ($LiOH{\cdot}H_2O$) were used to prepare 0.5 mol/L $(NH_4)_2S_2O_8$ and 2.0 mol/L LiOH solutions, respectively. The LiOH solution was gradually added to the $Mn(NO_3)_2$ solution with vigorous mixing, followed by 42.0 g of $LiOH{\cdot}H_2O$ until a white precipitate formed. The mixture was left at 25°C for 2 h, then heated to 80°C before $(NH_4)_2S_2O_8$ was added dropwise over 10 h. The black precipitate was filtered, washed, dried under vacuum at 120°C for 12 h, and sintered at 600°C for 24 h. Finally, the Li1.6Mn1.6O4 (LMO) powder was ground.

To form the granulated adsorbent, 3 g of chitosan was dissolved in 97 mL of 2% glacial acetic acid at room temperature. After achieving a uniform solution, 2 g of LMO was added and thoroughly mixed until a consistent black mixture was obtained. This mixture was then dispensed into a 1 mol/L NaOH solution using a needle-tipped syringe, resulting in spherical CTS/LMO granules. The granules were rinsed with deionized water until the pH stabilized at 7 and then dried at 60°C for 12 h.

To modify the adsorbent, 5 g of CTS/LMO was mixed with 75 mL of deionized water containing 0.075 g of NaCl and 0.35 mL of epichlorohydrin. After adding 0.3 g of KOH (dissolved in 2 mL of water) dropwise for 15 min, the mixture was stirred at 25°C for 16 h. The resulting solid was filtered, washed with distilled water, and dried overnight at 70°C.

CTS/HMO was prepared by shaking CTS/LMO in 0.25 M HCl for 12 h, replacing $Li^+$ with $H^+$ ions. This process caused the adsorbent to develop a slightly dark red/brown hue due to its manganese content. The mixture was then filtered, rinsed with deionized water until the pH stabilized at 4–5, and dried at 60°C for 12 h. The final adsorbent exhibited a uniform spherical shape with a diameter of approximately 1–2 mm.

Geothermal water samples with different physicochemical properties were collected from two locations in the geothermal-rich western Anatolia region of Türkiye: Germencik (Aydın) and Tuzla (Çanakkale) Geothermal Energy Power Plants. These water samples were characterized using various analytical methods, with detailed analysis results in Table 1.

## 2.2. Methods

### *2.2.1. Investigation of the effect of adsorbent dosage on Li recovery from geothermal waters*

The effect of CTS/HMO composite adsorbent dosage on Li recovery was investigated using water samples collected from the Germencik and Tuzla geothermal fields. Various amounts of adsorbent (0.05 g, 0.1 g, 0.2 g, 0.3 g, 0.4 g, and 0.5 g) were contacted with 25 mL geothermal water samples at 25°C in a water bath shaker operating at 180 rpm for 24 h. After 24 h, the adsorbent was filtered out, and the concentrations of Li were measured in the remaining solution using the ICP-OES instrument. Li recovery or separation efficiency percentages were calculated for each adsorbent dosage, and the optimal adsorbent amount was determined. The % Li separation efficiency was calculated using the following equation:

$$Li\ Recovery\ (\%) = [(C_0 - C_e)/C_0] \times 100 \qquad (1)$$

where $C_0$ represents the initial Li concentration in the geothermal water (mg/L), and $C_e$ denotes the equilibrium Li concentration after adsorption (mg/L).

The Li adsorption capacity ($q_e$, mg/g) is calculated using the equation:

$$q_e = [(C_0 - C_e) \times V]/m \qquad (2)$$

where $V$ is the volume of the solution (L), and $m$ is the amount of adsorbent used (g).

Moreover, the findings obtained from these studies were further analyzed using adsorption isotherms such as Langmuir, Freundlich, and Dubinin-Radushkevich (D-R), providing a theoretical explanation of the adsorption behavior.

**Table 1.** The physicochemical properties of the geothermal water sample collected from Germencik (Aydın) and Tuzla (Çanakkale) Geothermal Energy Power Plants

| **Cation species** | **Concentration (mg/L)** | | **Anion species** | **Concentration (mg/L)** | |
|---|---|---|---|---|---|
| | **Germencik** | **Tuzla** | | **Germencik** | **Tuzla** |
| [e]$Li^+$ | 6.56 | 32.27 | [b]$HCO_3^-$ | 1264.10 | 132.19 |
| [e]$Na^+$ | 1178.95 | 16920.53 | [a]$Cl^-$ | 1254.99 | 35170 |
| [e]$K^+$ | 80.24 | 2121.71 | [a]$F^-$ | 9.37 | 4.05 |
| [e]$Ca^{2+}$ | 14.75 | 2737.53 | [a]$NO_3^-$ | *N.D. | 4.64 |
| [e]$Mg^{2+}$ | 3.15 | 134.14 | [a]$SO_4^{2-}$ | 36.43 | 205.43 |
| [a]$NH_4^+$ | *N.D. | 105.19 | [a]$PO_4^{3-}$ | *N.D. | *N.D. |

| | **Germencik** | **Tuzla** |
|---|---|---|
| [c]pH | 8.94 | 6.71 |
| [d]Conductivity (mS/cm) | 2.79 | 83.4 |
| [d]Salinity (ppt) | 1.50 | 58.6 |
| [b]Total alkalinity (mg/L as $CaCO_3$) | 1036.15 | 108.36 |
| [e]B (mg/L) | 39.48 | 24.56 |
| [e]As (µg/L) | 110 | 37.11 |
| [f]$SiO_2$ (mg/L) | 152 | 230 |

[a]Ion chromatography (Thermo Scientific Dionex ICS-5000), [b]Titrimetric method, [c]pH meter (Thermo, Orion Star A111), [d]Multimeter (YSI Model 30M), [e]ICP-OES (Agilent Technologies, 5110), [f]Spectrophotometer (Hach-DR5000), *not determined (below the detection limit)

The Langmuir model postulates that adsorption occurs at distinct, homogeneous sites within the adsorbent, where each site can accommodate only a single $Li^+$ ion. Once occupied, no further adsorption can occur at that site. Additionally, the model assumes the absence of lateral movement of adsorbed species across the surface, leading to uniform adsorption energies [39,40]. The Langmuir isotherm model is given in Eq. (3), and to evaluate the favorability of adsorption for the Langmuir isotherm, the effect of the adsorption isotherm shape, was investigated using the dimensionless constant '$R_L$', also known as the separation factor or equilibrium parameter. The '$R_L$' value was calculated using Eq. (4) provided below, and if the value is between 0 and 1, the adsorption is favorable.

$$q_e = [(q_{max} K_L C_e)/(1 + K_L C_e)] \quad (3)$$

$$R_L = 1/(1 + K_L C_0) \quad (4)$$

where $q_{max}$ (mg/g) is the maximum adsorption capacity and $K_L$ (L/mg) is the Langmuir constant related to the affinity of the binding sites.

The Freundlich model is an empirical equation describing adsorption as an exponential function, where the adsorbate concentration on the adsorbent surface increases with rising bulk-phase concentration. This model suggests that adsorption initially occurs at the highest-affinity binding sites, with subsequent occupation of weaker sites as adsorption progresses. It characterizes sorption on heterogeneous surfaces or surfaces with sites of varying binding strengths [41]. The Freundlich isotherm is described in Eq. (5) as follows:

$$q_e = K_F {C_e}^{1/n} \quad (5)$$

where $K_F$ (L/g) and $n$ are Freundlich constants for the adsorption capacity and adsorption intensity of the adsorbent, respectively. The value of $n$ also describes the adsorption characteristics so that if $n>1$, the adsorption is favorable.

The D-R isotherm [42], as given in Equations 6, 7, and 8, allows for determining the nature of the adsorption process (physical or chemical) occurring on the surface of the adsorbent and can be used to calculate the mean free energy of adsorption ($E$). The value of this parameter helps determine the adsorption mechanism. If $E<8$ kJ/mol, the process is physical adsorption; if $8<E<16$ kJ/mol, the process is driven by ion exchange; and if $16<E<40$ kJ/mol, chemical adsorption occurs.

$$q_e = q_s exp(-\beta \varepsilon^2) \quad (6)$$

$$\varepsilon = [RTln(1 + 1/C_e)] \quad (7)$$

$$E = 1/(2\beta)^{0.5} \quad (8)$$

where $\beta$ is the model constant (mol²/kJ²), and $\varepsilon$ is the Polanyi potential (kJ/mol). T is the absolute temperature (K), and R (8.314 J/mol.K) is the related universal gas constant.

### 2.2.2. *Investigation of the effect of contact time on Li recovery from geothermal waters and adsorption kinetics*

The effect of contact time on Li recovery from geothermal waters and adsorption kinetics was studied by adding 3 g of adsorbent to 750 mL of geothermal water (4 g/L) and continuously stirring at 250 rpm. Samples of 5 mL were taken from the solution at specific time intervals (0, 5, 10, 15, 20, 30, 45, 60, 90, 120, 180, 240, 360, 480, and 1440 minutes) to evaluate the adsorption process.

The results obtained from the kinetic studies were evaluated using pseudo-first-order, pseudo-second-order, and intra-particle diffusion kinetic models.

The pseudo-first-order kinetic model [43] is given in Eq. (9):

$$ln(q_e - q_t) = lnq_e - k_1 t \quad (9)$$

where $q_e$ is the adsorption capacity at equilibrium (mg/g), $q_t$ is the adsorption capacity (mg/g) at time $t$ (h), and $k_1$ is the rate constant of the pseudo-first-order model (1/h).

The pseudo-second-order kinetic model related to equilibrium adsorption [44,45] is expressed in Eq. (10):

$$t/q_t = 1/(k_2 q_e^2) + t/q_e \quad 10)$$

where $k_2$ is the rate constant of the pseudo-second-order model (g/mg·h).

Since the kinetic models above cannot describe the diffusion mechanism, the intra-particle diffusion model, proposed by Weber and Morris [46], is an empirically derived functional relationship based on the theory expressed in Eq. (11):

$$q_t = k_{id} t^{0.5} + C_i \quad (11)$$

where $k_{id}$ is the intra-particle diffusion rate constant (mg/g·$h^{0.5}$), and $C_i$ is a constant related to the thickness of the boundary layer (mg/g).

### 2.2.3. *Adsorption selectivity of the CTS/HMO in geothermal waters*

The selectivity of the adsorbent to $Li^+$, $Na^+$, $K^+$, $Ca^{2+}$, and $Mg^{2+}$ was investigated from the experiment where 0.5 g of the CTS/HMO was contacted in 25 mL geothermal water samples at room temperature for 24 h. The distribution coefficient ($K_d$), separation factor ($\alpha_{Me}^{Li}$), and concentration factor (CF) were calculated considering $C_0$, $C_e$, and $q_e$ through Eq.'s 12 – 14 [28]:

$$K_d = (C_0 - C_e)V/(C_e V) \tag{12}$$

$$\alpha_{Me}^{Li} = K_{d_{Li}}/K_{d_{Me}} \tag{13}$$

$$CF = Q_{e_{Me}}/C_{0_{Me}} \tag{14}$$

### *2.2.4. Li recovery studies in a continuous-flow dynamic packed column system using a model solution*

A glass column with a diameter of 0.7 cm and a height of 12 cm, packed with CTS/HMO, was used for the chromatographic separation of Li from an aqueous solution. A continuous-flow packed column system was employed to investigate Li sorption using a solution with an initial Li concentration of 10 mg/L. The solution was fed from top to bottom at a flow rate of 0.25 mL/min through a column with a bed height of 1.5 cm. Li sorption experiments were conducted using a peristaltic pump (SHENCHEN model) and a fraction collector (BÜCHI C-660), with 3 mL fractions collected, as illustrated in Fig. 1. Li desorption experiments were performed using a 5% (v/v) $H_2SO_4$ solution at a flow rate of 0.12 mL/min, with 2 mL fractions collected. The Li concentration in the samples was also determined using an ICP-OES instrument (Agilent Technologies, 5110).

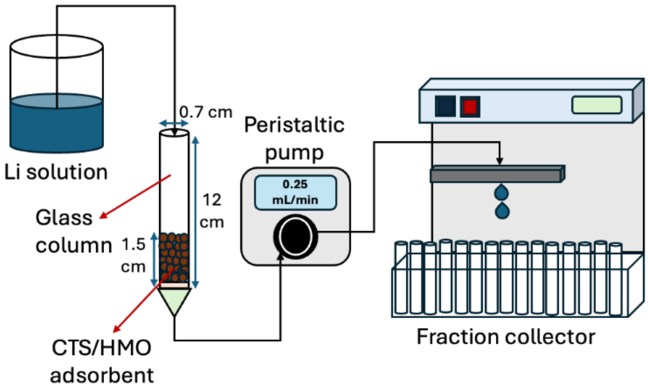

**Figure 1.** Schematic illustration of chromatographic separation set-up

The breakthrough curves representing the performance of fixed-bed column sorption were plotted as normalized concentration ($C/C_0$), defined as the ratio of the effluent Li concentration (C, mg/L) to the influent Li concentration ($C_0$, mg/L), against the bed volume. The bed volume (BV, mL solution/mL adsorbent) was calculated using Eq. (15) [47]:

$$BV = Q.t/V \tag{15}$$

where $Q$ represents the feed solution flow rate (mL/min), $t$ is the operation time (min), and $V$ is the wet volume of the adsorbent (mL).

The breakthrough time ($t_b$) and breakthrough capacity are critical parameters in column adsorption processes, where the breakthrough time represents the operational lifespan of the adsorbent in a single adsorption cycle. Typically, the breakthrough time is defined based on the ratio of the effluent concentration to the influent concentration. For example, the breakthrough time is commonly taken in heavy metal removal when the effluent concentration reaches 5% of the feed concentration ($C/C_0 = 0.05$). However, since this study focuses on recovering a valuable metal, $t_b$ is defined based on the Li extraction efficiency, following literature recommendations [48]. Specifically, the $t_b$ is taken as the time required for the Li extraction efficiency to decrease to 60%, corresponding to an effluent concentration of approximately 4 mg/L from an initial feed concentration of 10 mg/L.

The total or stoichiometric capacity of the bed and the usable capacity of the bed up to the break-point (breakthrough) time $t_b$ of the bed are calculated by Eq. (16) and Eq. (17), respectively [49]:

$$t_t = \int_0^\infty (1 - C/C_0)\,dt \tag{16}$$

$$t_u = \int_0^{t_b} (1 - C/C_0)\,dt \tag{17}$$

where $t_t$ is the time equivalent to the total or stoichiometric capacity, and $t_u$ is the time equivalent to the usable capacity or when the effluent concentration reaches its maximum permissible level. The value of $t_u$ is usually very close to that of $t_b$. Numerical integration of Eqs. (16) and (17) was done using a spreadsheet.

The scale-up design method was applied to estimate the length of bed used up to the breakpoint, $H_B$ (Eq. (18)), and the length of unused bed, $H_{UNB}$ (Eq. (19)), for a total bed length of $H_T$ (Eq. (20)), simulating a full-scale packed-bed tower [49].

$$H_B = (t_u/t_t)H_T \tag{18}$$

$$H_{UNB} = (1 - t_u/t_t)H_T \tag{19}$$

$$H_T = H_B + H_{UNB} \tag{20}$$

The $H_{UNB}$ represents the mass transfer zone (MTZ), primarily influenced by fluid velocity rather than the total column length. To determine $H_{UNB}$, experiments can be conducted in a small-diameter laboratory column packed with the chosen adsorbent at the design velocity. When scaling up to a full-scale adsorption system, the total bed height ($H_T$) is calculated by adding the $H_{UNB}$ to the bed height required to achieve the desired adsorption capacity at the breakpoint ($H_B$). This approach allows for an efficient transition from laboratory-scale testing to industrial-scale application [49].

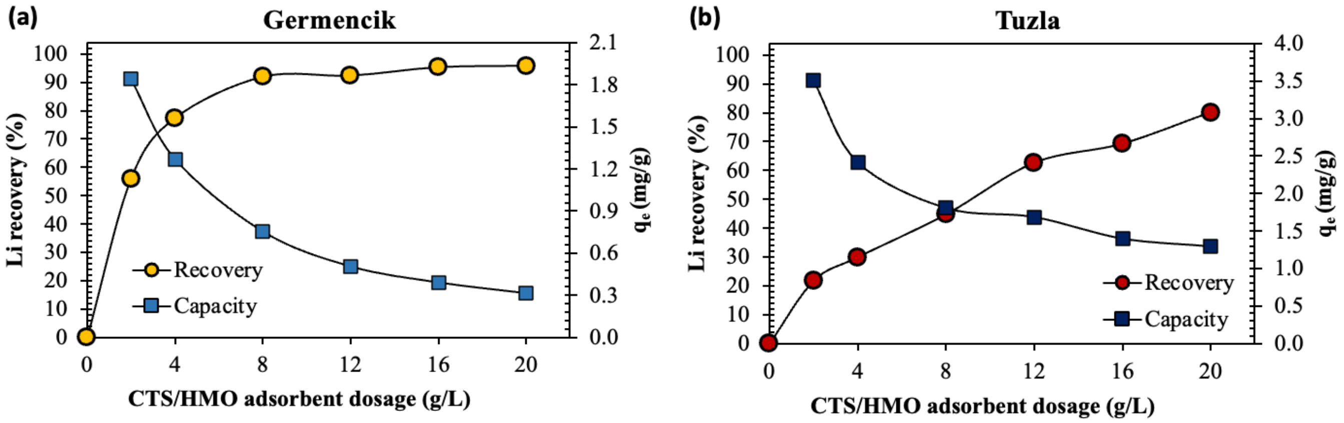

**Figure 2.** The effect of CTS/HMO adsorbent dose on Li recovery and the adsorption capacity using (a) Germencik and (b) Tuzla geothermal waters

## 3. Result and discussion

### 3.1. Characteristics of the adsorbent

As we reported previously, the characteristics of the synthesized adsorbent were discussed in detail [38]. For example, EDX integrated with SEM analysis of CTS/HMO confirmed the presence of C and O from the raw chitosan structure and the uniform incorporation of Mn into both CTS/LMO and the final CTS/HMO product. The even distribution of Mn indicated a homogeneous functional structure throughout the composite. Additionally, the elemental composition—31.22% C, 44.36% O, and 15.62% Mn—validated the successful synthesis.

The FTIR spectrum of chitosan showed O–H and N–H stretching (3250–3500 cm$^{-1}$) and peaks for –$NH_2$ deformation (1650 cm$^{-1}$) and C–N stretching (1380 cm$^{-1}$). LMO exhibited a Li–O absorption band at 530 cm$^{-1}$, with $MnO_6$ and $LiO_6$ groups shifting the Mn–O peak from 633 cm$^{-1}$ to 901 cm$^{-1}$. In CTS/LMO and CTS/HMO, reduced peak intensity confirmed successful cross-linking. The absence of Li–O vibrations (500–550 cm$^{-1}$) in CTS/HMO indicated $Li^+$ to $H^+$ conversion. Lithium removal caused spectral changes, producing peaks at 520, 495, 605, and 325 cm$^{-1}$, while cubic symmetry was maintained.

The XRD diffractogram of chitosan displayed broad peaks at $2\theta = 10°$ and $20°$, but in CTS/LMO and CTS/HMO, the 10° peak disappeared, and the 20° peak weakened, confirming chitosan's compatibility with LMO. Diffractograms matched standard references, verifying successful LMO synthesis. Characteristic peaks at $2\theta = 18.69°$, 36.40°, 38.10°, 44.29°, 48.66°, 58.73°, 64.55°, and 67.83° corresponded to $Li_{1.6}Mn_{1.6}O_4$ crystal planes. Cross-linking with epichlorohydrin reduced peak intensities due to increased amorphicity, though LMO spinel peaks remained. Acid-treated CTS/HMO showed further intensity reduction, indicating successful chitosan coating on LMO.

The specific surface area of LMO was measured by BET analysis at 8.410 m$^2$/g. In contrast, the surface area of CTS/HMO significantly dropped to 0.185 m$^2$/g due to increased particle size from LMO granulation with cross-linked chitosan. This decrease is likely due to reduced porosity caused by chitosan covering the lattice and collapsing pores.

The adsorption mechanism of the CTS/HMO depends on the $Li^+/H^+$ ion exchange and it is provided in the chemical equation below:

$$H_{1.6}Mn_{1.6}O_4 + Li^+ \rightleftharpoons Li_{1.6}Mn_{1.6}O_4 + H^+$$

### 3.2. Determination of optimum adsorbent dose and adsorption isotherms

The comparative graph of the Li recovery efficiency and the static adsorption capacity against the adsorbent dose for both Germencik and Tuzla geothermal waters is shown in Fig. 2(a) and Fig 2(b), respectively. As the adsorbent amount increased, the number of functional groups available for Li adsorption also increased, resulting in an enhanced Li recovery rate. For Germencik, the Li recovery rapidly increased with the rise in adsorbent dose, reaching over 90% recovery at a dose of 8 g/L. However, with further increases beyond 8 g/L, the recovery rate slowed, and after 12 g/L, it plateaued at around 95%. This indicates that adding more adsorbent does not yield further benefits. Therefore, the optimum adsorbent dose for effective Li recovery from Germencik geothermal water was 0.2 g/25 mL of geothermal water (8 g/L). For Tuzla, Li recovery started at lower levels and reached approximately 65% at a dose of 12 g/L. After 12 g/L, the recovery rate increased more slowly and approached 80% at a dose of 20 g/L. This indicates that more adsorbent is required for Li recovery from Tuzla water. This is because, while Germencik geothermal water contains 6.56 mg/L of Li, Tuzla geothermal water has a higher Li concentration of 32.27 mg/L and a more saline characteristic than Germencik. On the other hand, despite Germencik having nearly one-fifth less Li, its softer characteristics

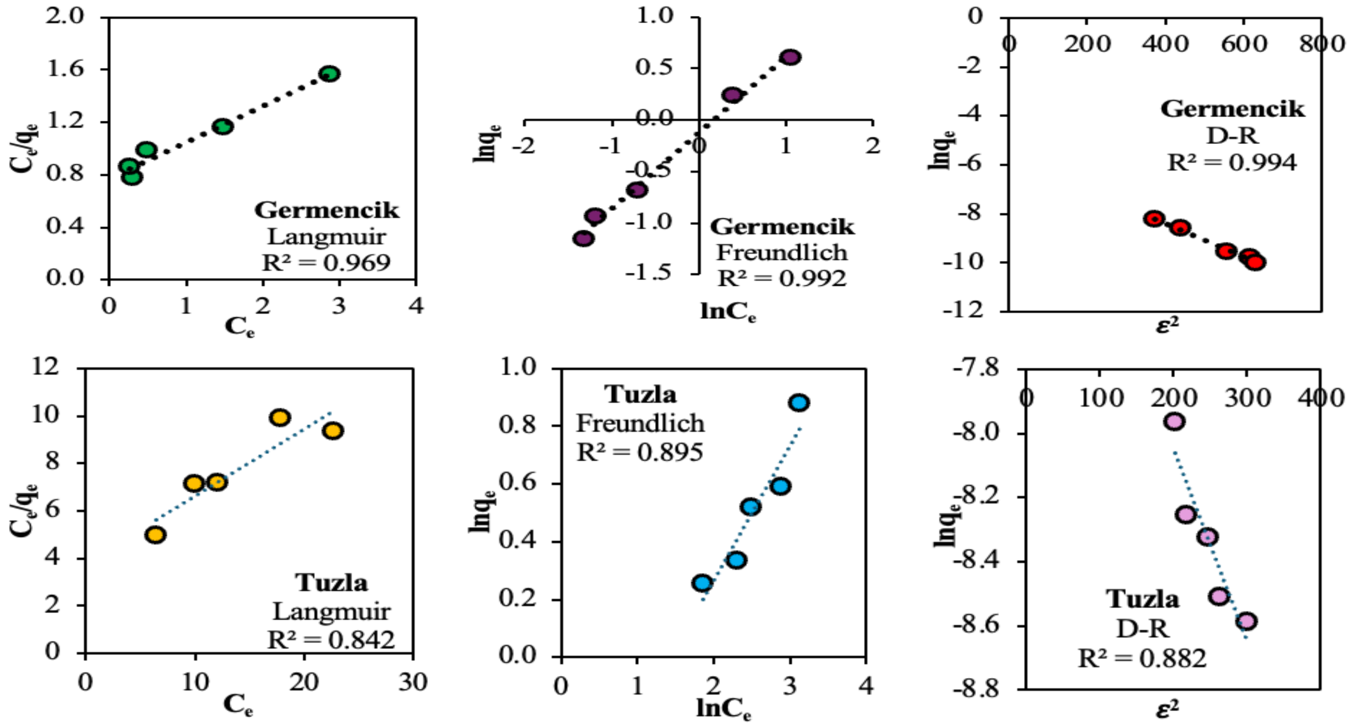

**Figure 3.** The trend lines of the experimental data for the adsorption behavior of Li from Germencik and Tuzla geothermal water onto CTS/HMO using Langmuir, Freundlich, and Dubinin-Radushkevich (D-R) type isotherms

allow for a higher Li recovery of 95%, while the aforementioned factors can explain the lower recovery rate for Tuzla geothermal water. Furthermore, the maximum static adsorption of lithium onto CTS/HMO adsorbent was achieved for an adsorbent-to-solution ratio of 2.0 g/L, as expected. It was found to be 1.84 mg/g for Germencik geothermal water, while it was 3.51 mg/g for Tuzla geothermal water.

Furthermore, the adsorption equilibrium is typically characterized by an isotherm equation that describes the affinity and surface properties of the adsorbent under specific pH and temperature conditions. These equations establish the relationship between the amount of adsorbate bound to the adsorbent and the concentration of the dissolved adsorbate in the liquid phase, which are referred to as adsorption isotherms.

Adsorption isotherms help characterize any pollutant removal or valuable metal recovery process using an adsorbent and distinguish between physical/chemical phenomena, favorable adsorption, adsorption energy, and single-layer versus multi-layer adsorption scenarios. These equations are generally used to describe experimental isotherms and were developed by Freundlich, Langmuir, and Dubinin-Radushkevich (D-R).

Fig. 3 shows the linear fitting of isotherm models with experimental data for Germencik and Tuzla geothermal waters, providing information on the adsorption

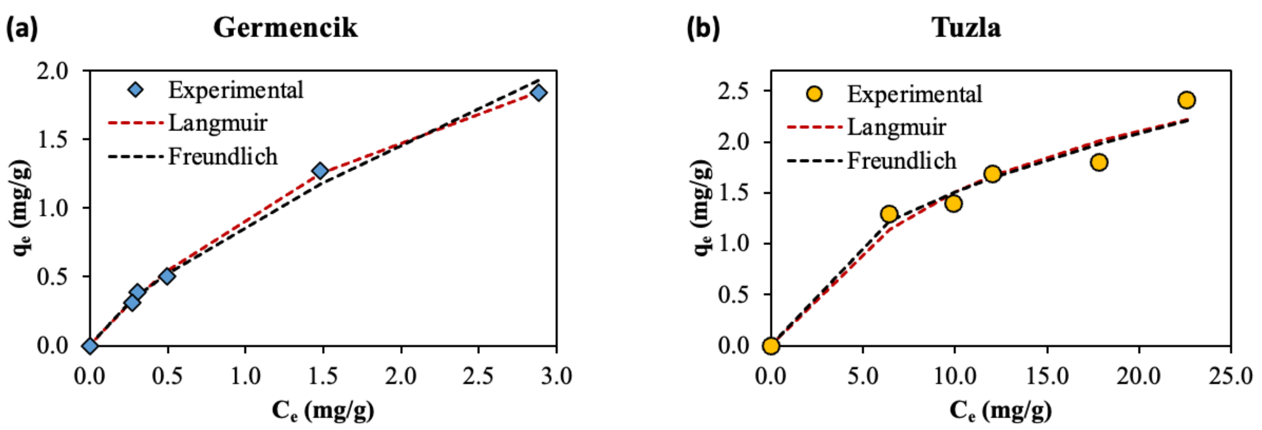

**Figure 4.** Comparison of lithium adsorption isotherm fitting and experimental data using CTS/HMO for **(a)** Germencik and **(b)** Tuzla geothermal waters

behavior of $Li^+$ ions with CTS/HMO. Fig. 4(a) and Fig. 4(b) are $q_e$ vs. $C_e$ plots for the experimental and theoretical data reproduced by Langmuir and Freundlich isotherms for lithium recovery from Germencik and Tuzla geothermal waters, respectively, using CTS/HMO adsorbent. Table 2 includes the isotherm model equations, associated parameters, and their values.

**Table 2**. The values of the isotherm models and associated parameters for Li adsorption from Germencik and Tuzla geothermal waters using the CTS/HMO adsorbent

| **Isotherm model** | **Linear form** | **Parameters** | **Values** | |
|---|---|---|---|---|
| | | | **Germencik** | **Tuzla** |
| Langmuir | $\frac{C_e}{q_e} = \frac{1}{q_{max}} C_e + \frac{1}{K_L q_{max}}$ | $q_{max}$ (mg g$^{-1}$) | 3.622 | 3.556 |
| | | $K_L$ (L mg$^{-1}$) | 0.358 | 0.073 |
| | | $R^2$ | 0.969 | 0.842 |
| Freundlich | $ln q_e = \frac{1}{n} ln C_e + ln K_F$ | $K_F$ (L/g) | 0.881 | 0.510 |
| | | n | 1.350 | 2.128 |
| | | $R^2$ | 0.992 | 0.895 |
| D-R | $ln q_e = -\beta \varepsilon^2 + ln q_s$ | β (mol$^2$ kJ$^{-2}$) | 0.0067 | 0.0060 |
| | | E (kJ mol$^{-1}$) | 8.64 | 9.13 |
| | | $q_s$ (mg g$^{-1}$) | 22.88 | 7.33 |
| | | $R^2$ | 0.994 | 0.882 |

The experimental dataset shows strong compatibility with the Langmuir model, but due to the higher correlation coefficient of the graph plotted between $lnq_e$ and $lnC_e$, it can be concluded that CTS/HMO adsorbent exhibits Freundlich-type adsorption behavior for Li in both Germencik ($R^2$ = 0.992) and Tuzla ($R^2$ = 0.895) geothermal waters. The Freundlich constants, *n*, and $K_F$, were found to be 1.350 and 0.881 for Germencik geothermal water and 2.128 and 0.510 for Tuzla geothermal water, respectively. *n* values greater than 1 suggest that $Li^+$ ions are favorably adsorbed by the adsorbent, and the adherence to the Freundlich isotherm indicates that the adsorbent may have a heterogeneous structure.

The $C_e/q_e$ vs. $C_e$ graphs showing the adsorption of $Li^+$ ions onto CTS/HMO adsorbent displayed linear relationships with high correlation coefficients, confirming that the Langmuir model applies to the current study. The monolayer maximum adsorption capacity ($q_{max}$) and Langmuir constant ($K_L$) values were found to be 3.622 mg/g and 0.358 for Germencik geothermal water and 3.556 mg/g and 0.0073 for Tuzla geothermal water, respectively. Compared to the experimental equilibrium capacity ($q_e$) values (1.571 mg/g and 2.073 mg/g) under specific conditions, the $q_{max}$ values from the Langmuir isotherm did not match closely. These findings suggest that instead of $Li^+$ ions adsorbing in a monolayer homogeneous configuration, a multilayer heterogeneous adsorption process occurs on the CTS/HMO surface, validating the Freundlich-type adsorption behavior. Additionally, the effect of the isotherm shape on the feasibility of adsorption was investigated for the Langmuir isotherm. On the other hand, the obtained $R_L$ values, which range between 0 and 1, confirm that the adsorption process is favorable for both Germencik and Tuzla geothermal waters. This result is also strongly supported by the *1/n* values obtained from the Freundlich isotherm.

According to the D-R isotherm model, the *E* value for Li adsorption from Germencik geothermal water was determined to be 8.64 kJ/mol, and for Tuzla geothermal water, it was 9.13 kJ/mol. This suggests that ion exchange governs the adsorption mechanism of $Li^+$ ions onto the CTS/HMO adsorbent. The value of the $q_s$ parameter in the model (22.88 mg/g for Germencik and 7.33 mg/g for Tuzla) reflects the porosity of the adsorbent: the larger this value compared to the equilibrium capacity, the more developed the active binding sites are.

### 3.3. The effect of contact time and adsorption kinetics

The Li recovery efficiency from Germencik and Tuzla geothermal water over time is illustrated in Fig. 5(a) as a $C/C_0$ vs. time graph and in Fig. 5(b) as a $q_e$ vs. time graph. The adsorption kinetics for both geothermal waters showed an initially rapid Li recovery rate, gradually slowing down before reaching equilibrium for Li adsorption onto the CTS/HMO adsorbent. With a 4 g/L

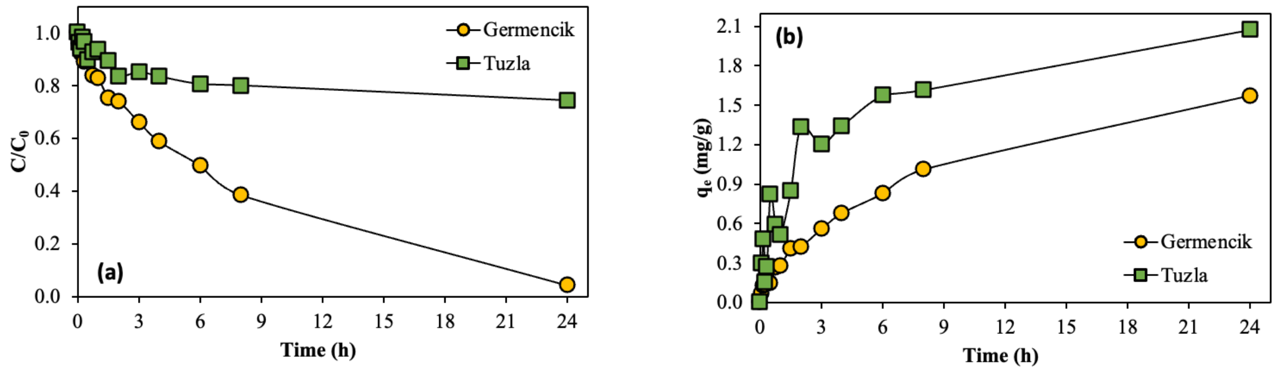

**Figure 5.** The effect of contact time on Li recovery from Germencik and Tuzla geothermal waters in terms of (a) normalized concentration ($C/C_0$) vs. time and (b) adsorption capacity ($q_e$, mg/g) vs. time

adsorbent dose, equilibrium was achieved after 24 h, with approximately 95% Li recovery efficiency from Germencik geothermal water and about 25% from Tuzla geothermal water. Despite a lower Li recovery percentage for Tuzla water due to its high salt content, the increased mass transfer caused by a stronger concentration polarization effect resulted in a Li adsorption capacity of 2.073 mg/g. In comparison, the adsorption capacity for Germencik geothermal water was determined to be 1.571 mg/g under given conditions.

**Table 3.** The calculated parameters and correlation coefficients of the kinetic models for Li recovery from Germencik and Tuzla geothermal waters using the CTS/HMO adsorbent

| **Kinetic model** | | **Germencik** | **Tuzla** |
|---|---|---|---|
| Pseudo-first order | $R^2$ | 0.992 | 0.875 |
| | $q_e$,theo (mg/g) | 1.460 | 1.638 |
| | $k_1$ ($h^{-1}$) | 0.119 | 0.185 |
| | $q_{e,}$ exp (mg/g) | 1.571 | 2.073 |
| Pseudo-second order | $R^2$ | 0.898 | 0.914 |
| | $q_e$,theo (mg/g) | 1.201 | 1.914 |
| | $k_2$ (g $mg^{-1}$ $h^{-1}$) | 0.321 | 0.342 |
| | $q_{e,}$ exp (mg/g) | 1.571 | 2.073 |
| Inrtaparticle diffuision | $R^2$ | 0.991 | 0.868 |
| | $k_i$ (g $mg^{-1}$ $h^{-0.5}$) | 0.365 | 0.588 |

Moreover, Fig. 6 presents the linear graphs of the three kinetic models, as the pseudo-first-order, pseudo-second-order, and intraparticle diffusion models, illustrating their alignment with the experimental data for both Germencik and Tuzla geothermal waters. The linear equations and correlation coefficients ($R^2$) demonstrate the compatibility. When the correlation coefficients of the pseudo-first-order and pseudo-second-order kinetic models evaluated separately for the CTS/HMO adsorbent in Table 3 are compared, it was determined that Li adsorption from Germencik geothermal water fits the pseudo-first-order kinetic model. In contrast, Li adsorption from Tuzla geothermal water fits the pseudo-second-order model, as the coefficients are higher. Additionally, the kinetic parameters for each model were calculated. Furthermore, when the theoretical adsorption capacity (qe, theoretical, mg/g) was compared with the experimentally determined adsorption capacity, it was observed that the deviation was smaller for the kinetic model, showing better agreement. The rate constants for adsorption kinetics were calculated as 0.119 h-1 and 0.342 g mg-1 h-1 for Germencik and Tuzla geothermal waters, respectively.

When interpreting experimental kinetic data, determining the rate-limiting step is crucial from a mechanistic perspective. The transport of the adsorbate to the adsorbent surface involves multiple stages. For instance, in Li adsorption, three main steps are typically observed: transport of Li to the surface (film diffusion), transport within the pores of the adsorbent (particle diffusion), and adsorption onto the inner surfaces of the pores. The final step is generally rapid and does not determine the overall rate. The slowest step, which could be either film diffusion or pore diffusion, dictates the overall adsorption rate. However, the controlling step can vary depending on the external mass transfer and intraparticle diffusion mechanisms. External mass transfer dominates in systems with poor mixing, low adsorbate concentrations, small adsorbent particle sizes, and high adsorbate affinity for the adsorbent. Conversely, intraparticle diffusion becomes significant in well-mixed systems with larger adsorbent particle sizes, higher adsorbate concentrations, and lower adsorbate affinity for the adsorbent.

The most common method for distinguishing adsorption mechanisms is fitting experimental data to the intraparticle diffusion model proposed by Weber and Morris in 1962 (Eq. (11)). In many cases documented in the literature, multiple linearities have been observed in the qt versus t0.5 plot. However, as shown in Fig. 6, the adsorption data of Li onto CTS/HMO for Tuzla geothermal water, despite some deviations, was represented by a single straight line. This suggests the dominance of external diffusion (boundary layer diffusion). Nevertheless, the data points do not intercept the origin, indicating that boundary layer diffusion is not the sole limiting mechanism and that other factors, such as repulsive forces between Li+ ions and the adsorbent (due to concentration gradients), also significantly contribute. The intercept, Ci, provides information about the boundary layer thickness: a higher intercept indicates a more pronounced boundary layer effect. The Ci value was found to be 0.13 mg/g. Moreover, the intraparticle diffusion rate constant, derived from the slope of the qt versus t0.5 plot, was determined to be 0.365 mg/g h0.5 for Germencik geothermal water and 0.588 mg/g h0.5 for Tuzla geothermal water.

So far, the adsorption of Li from reverse osmosis (RO) concentrate of geothermal water has been studied using powdered and granulated forms of Li-selective spinel-type manganese oxide (λ-MnO2) adsorbents. The interaction between Li+ ions and λ-MnO2 was examined through equilibrium and kinetic studies, focusing on adsorption capacity and uptake rate. The Langmuir isotherm model effectively described the adsorption of Li+ ions ($q_{max}$: 33.44 mg/g and 27.40 mg/g), and the pseudo-second-order kinetic model ($k_2$: 0.2912 g/mg.min and 0.0030 g/mg.min) best represented the lithium uptake process by both forms of $\lambda$-Mn$O_2$ [50].

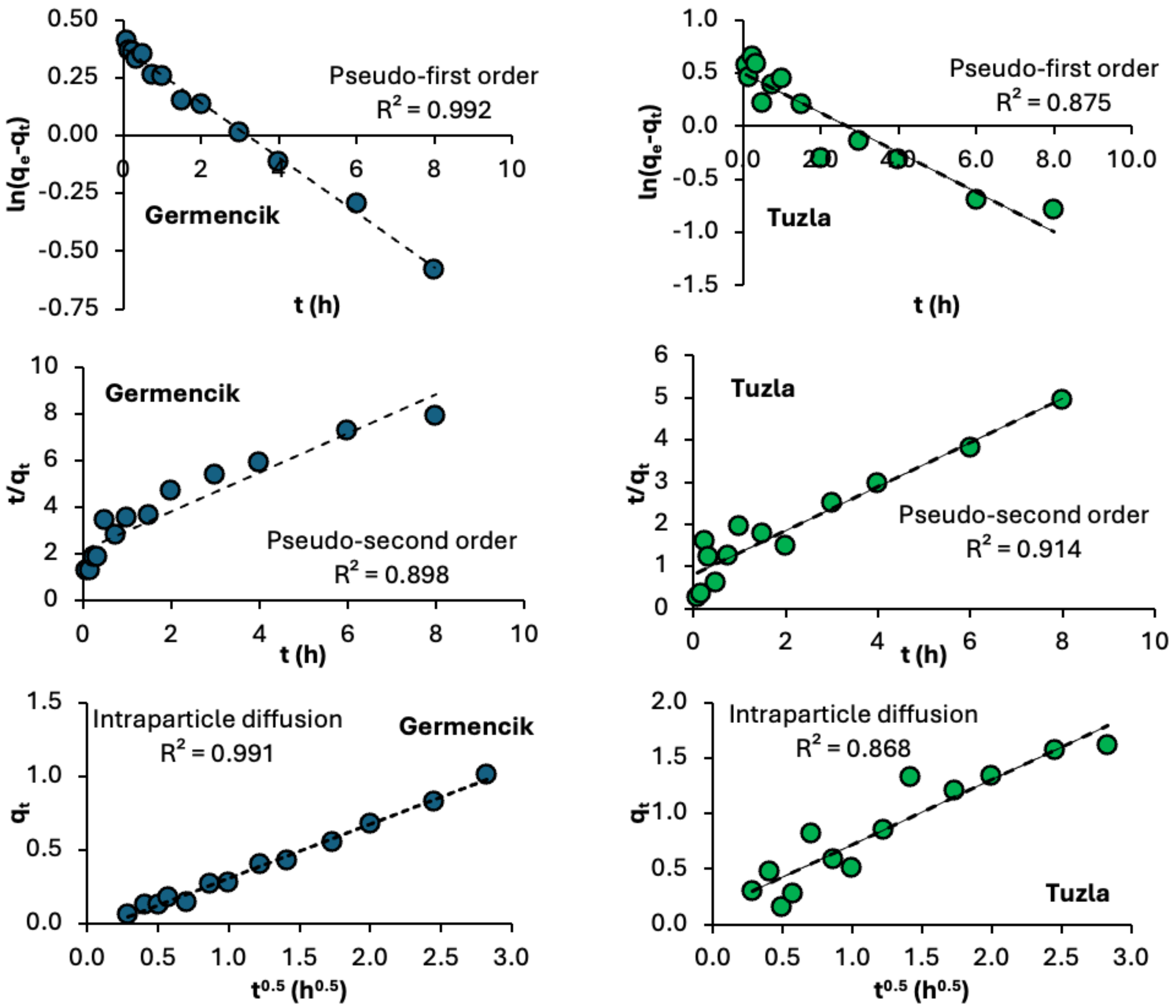

**Figure 6.** The trend lines of experimental data for Germencik and Tuzla geothermal waters, investigating the adsorption behavior of Li onto CTS/HMO, were analyzed using pseudo-first-order, pseudo-second-order, and intraparticle diffusion kinetic models

### 3.4. Selectivity of the CTS/HMO adsorbent

The selectivity of the adsorbent toward $Li^+$ relative to competing cations can be assessed by examining the distribution coefficient ($K_d$) and selectivity coefficient ($\alpha_{Me}^{Li}$), while the concentration factor (CF) provides a measure of Li enrichment efficiency and the obtained results are given in Table 4. In the Germencik geothermal water, the $K_d$ value for $Li^+$ (1.166 mL/g) is substantially higher than those of $Na^+$ (0.001 mL/g), $K^+$ (0.001 mL/g), $Ca^{2+}$ (0.002 mL/g), and $Mg^{2+}$ (0.003 mL/g), reflecting strong preferential adsorption of $Li^+$ over these competing ions. This is further supported by the high $Mg^{2+}/Li^+$ selectivity coefficient ( $\alpha_{Mg^{2+}}^{Li^+}$ = 380.66), underscoring the minimal interference of $Mg^{2+}$ in lithium uptake.

In contrast, the Tuzla geothermal water exhibits a notably lower $K_d$ for $Li^+$ (0.201 mL/g), with comparable values for competing cations. Yet, the $Mg^{2+}/Li^+$ selectivity coefficient significantly declines to 58.88, indicating a reduced capacity of the adsorbent to distinguish between these ions under the given conditions. The CF further substantiates these findings, with Germencik exhibiting a higher lithium enrichment efficiency (CF = 47.943 L/g × $10^{-3}$) than Tuzla (CF = 40.037 L/g × $10^{-3}$). The relatively lower CF values for competing cations, particularly $Na^+$ (0.610 L/g × $10^{-3}$) and $Mg^{2+}$ (2.885 L/g ×

**Table 4.** Adsorption selectivity of the CTS/HMO in Germencik and Tuzla geothermal water

| | C0 (mg/L) | | Ce (mg/L) | | qe (mg/g) | | CF (L/g x $10^{-3}$) | | Kd (mL/g) | | $\alpha_{Me}^{Li}$ | |
|---|---|---|---|---|---|---|---|---|---|---|---|---|
| Ion | Germencik | Tuzla | Germencik | Tuzla | Germencik | Tuzla | Germencik | Tuzla | Germencik | Tuzla | Germencik | Tuzla |
| $Li^+$ | 6.56 | 32.27 | 0.270 | 6.430 | 0.315 | 1.292 | 47.94 | 40.037 | 1.166 | 0.201 | 1.00 | 1.00 |
| $Na^+$ | 1178.95 | 16920.53 | 1164.57 | 15977.4 | 0.719 | 47.156 | 0.610 | 2.787 | 0.001 | 0.003 | 1887.33 | 68.08 |
| $K^+$ | 80.24 | 2121.71 | 79.134 | 2060.53 | 0.055 | 3.059 | 0.686 | 1.442 | 0.001 | 0.001 | 1675.48 | 135.35 |
| $Ca^{2+}$ | 14.75 | 2737.53 | 14.079 | 2573.7 | 0.034 | 8.1915 | 2.281 | 2.992 | 0.002 | 0.003 | 487.66 | 63.13 |
| $Mg^{2+}$ | 3.15 | 134.14 | 2.972 | 125.570 | 0.009 | 0.4285 | 2.885 | 3.194 | 0.003 | 0.003 | 380.66 | 58.88 |

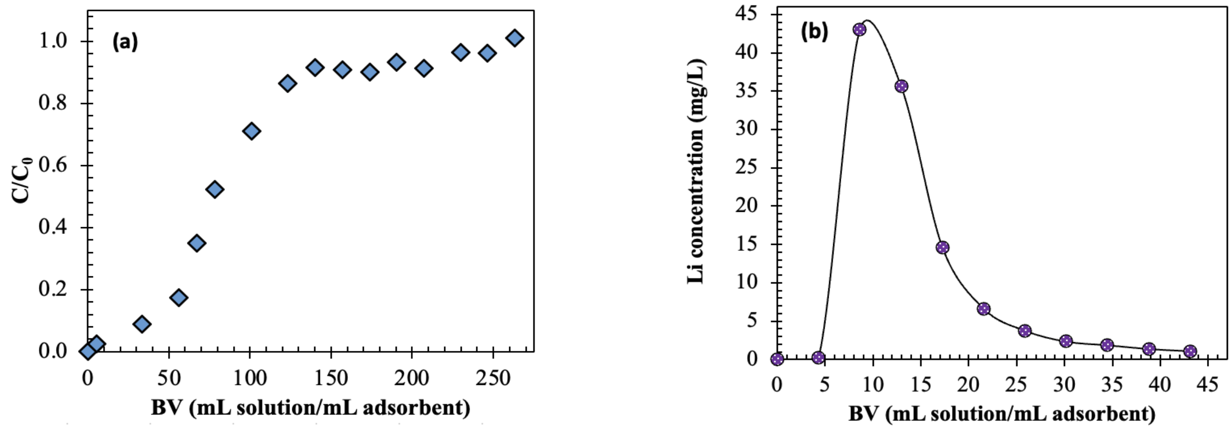

**Figure 7.** Concentration profiles for the packed bed column by CTS/HMO for Li **(a)** breakthrough curve ($C_0$=10 mg/L, $pH_{initial}$=12, T=25°C, bed height=1.5 cm, $\vartheta$=0.25 mL/min) and **(b)** elution curve (5% $H_2SO_4$, $\vartheta$=0.12 mL/min, T=25°C)

$10^{-3}$) in Germencik, suggest that the adsorbent operates with greater specificity in this system. Conversely, in Tuzla, the increased CF values for $Na^+$ (2.787 L/g × $10^{-3}$), $Mg^{2+}$ (3.194 L/g × $10^{-3}$), and other cations point to a more competitive adsorption environment, which may be attributed to the elevated ionic strength and complex geochemical composition of this geothermal brine. Overall, the results demonstrate that while the adsorbent exhibits a strong affinity for lithium in both geothermal sources, its performance is significantly influenced by the competing ion matrix, with Germencik offering a more favorable environment for selective lithium recovery.

### 3.5. Fixed-bed adsorption/desorption concentration profiles and capacity of the column

The chromatographic separation of Li from aqueous solution using CTS/HMO adsorbent was demonstrated through breakthrough and desorption curves, as shown in Fig. 7(a) and Fig. 7(b). During adsorption, the initial $C/C_0$ value was close to zero, indicating effective Li uptake. As BV increased, $C/C_0$ gradually rose, reaching approximately 0.9 at 140 BV, signifying near-saturation of the adsorbent. At 241 BV, $C/C_0$ reached 1.0, confirming complete saturation. The breakthrough point, defined as the time when lithium extraction efficiency dropped to 60%, resulted in a breakthrough capacity of 0.435 mg Li/mL adsorbent at 67 BV. At saturation, the total capacity was determined as 0.63 mg Li/mL adsorbent at 241 BV, with a column utilization efficiency of 69.03%.

A sharp peak of approximately 43 mg/L was observed during the desorption phase at 9 BV, indicating rapid and efficient Li desorption. The concentration then declined swiftly, falling below 10 mg/L at 22 BV and approaching 1 mg/L after 43 BV. These results demonstrate that the CTS/HMO adsorbent can effectively retain Li up to 241 BV and subsequently release it in a concentrated form. The majority of Li was recovered within the first 17 BV of the elution solution, with an elution efficiency of 76%. 0.25 M HCl could be used instead of 5% $H_2SO_4$ in batch desorption and conditioning processes to enhance this efficiency.

On the other hand, the time equivalent to the usable capacity was found to be 144 min, and the length of the used bed was 1.02 cm. The total saturation time was 212 min, resulting in 0.48 cm of unused bed. Mass transfer limitations, including film and pore diffusion, slowed adsorption, leading to a gradual increase in $C/C_0$ rather than a sharp transition. The particle size-to-column diameter ratio also influenced bed porosity, further impacting breakthrough curve behavior. Enhancing adsorption efficiency in dynamic column operations requires optimization of key parameters such as column configuration, flow rate, pH, and temperature. Adjusting the height-to-diameter ratio and adsorbent packing density increases residence time, ensuring effective interaction between the solution and adsorbent. Pulsed or variable flow regimes optimize Li uptake by extending residence time, while precise pH control enhances Li selectivity [51]. Sustainable adsorption-regeneration cycles and real-time monitoring improve process efficiency and ensure consistent Li recovery under varying operational conditions.

Table 5 summarizes key findings from this study, including adsorption capacity, desorption efficiency, and degree of column utilization (breakthrough capacity/total capacity) under the investigated conditions using CTS/HMO.

**Table 5.** Fixed bed column operation results for Li recovery using CTS/HMO adsorbent

| | |
|---|---|
| Breakthrough capacity, mg Li/mL adsorbent | 0.435 |
| Breakpoint time, $t_b$, min | 144 |
| BV at breakthrough capacity, mL solution/mL adsorbent | 67 |
| Total capacity, mg Li/mL adsorbent | 0.630 |
| Total saturation time, $t_t$, min | 212 |
| BV at total capacity, mL solution/mL adsorbent | 241 |
| Degree of column utilization, % | 69.03 |
| Elution efficiency, % | 75.72 |
| Used bed length, $H_B$, cm | 1.02 |
| Unused bed length, $H_{UNB}$, cm | 0.48 |

Recently, electrolytic manganese dioxide ($\gamma$-$MnO_2$) powder was tested as a sorbent for Li recovery from geothermal water obtained from the Tuzla Geothermal Power Plant (GPP). The sorption and desorption behavior of $\gamma$-$MnO_2$ was evaluated under various conditions, including sorption at 360 K and 2 bars. The highest sorption efficiency was achieved after 1 h of treatment with Tuzla GPP brine. For desorption, acidic solutions were used, and the average concentration of Li in the desorption solution was 25 mg/L when 10 g of $\gamma$-$MnO_2$ was added to 30 mL of the acidic solution. After four cycles, the desorption process was repeated using the same solution for cumulative Li recovery, reaching a Li concentration of 230 mg/L [52]. Table 6 also compares some adsorbents available in the literature regarding Li source and adsorption capacity.

**Table 6.** Comparison of some adsorbents available in the literature regarding lithium source and their maximum adsorption capacity

| Adsorbent | Li source | $q_{max}$ (mg/g) | Ref. |
|---|---|---|---|
| $Li_{1.6}Mn_{1.6}O_4$ | Seawater | 40 | [53] |
| Powder $\lambda$-$MnO_2$ | RO concentrate of geothermal water | 33.44 | [50] |
| Granulated $\lambda$-$MnO_2$ | | 27.40 | |
| Powder $\lambda$-$MnO_2$ | Balçova geothermal water | 31.55 | [30] |
| Granulated $\lambda$-$MnO_2$ | | 30.42 | |
| $HZn_{0.5}Mn_{1.5}O_4$ | Artifical seawater | 33.1 | [54] |
| $Li_{1.6}Mn_{1.6}O_4$ | Qarhan Salt Lake brine | 26.93 | [55] |
| $Li_{1.6}Mn_{1.6-x}Cr_xO_4$ | Lop Nor Salt Lake | 25.5 | [56] |
| Lewatit TP-260 ion exchange resin | Germencik geothermal water | 4.31 | [4] |
| CTS/HMO | Model Li solution ($C_0$=10 mg/L) | 4.94 | [38] |
| CTS/HMO | Germencik geothermal water | 3.62 | This study |
| | Tuzla geothermal water | 3.56 | |

## 4. Conclusions

The study demonstrated the efficacy of the CTS/HMO composite as a promising adsorbent for Li recovery from geothermal brines, leveraging the distinctive physicochemical properties of geothermal waters from Germencik and Tuzla in the western region of Türkiye. The adsorption process, underpinned by Freundlich-type multilayer and heterogeneous adsorption behavior, showcased the versatility of the material in accommodating variable ionic compositions. Notably, the kinetic studies revealed a distinct dependence of adsorption dynamics on the brine source, with Li adsorption aligning with pseudo-first-order kinetics for Germencik geothermal water and pseudo-second-order kinetics for Tuzla geothermal water. These differences highlight the critical role of geothermal water characteristics, such as salinity and Li concentration, in influencing adsorption mechanisms. The D-R model provided insights into adsorption behavior, suggesting ion exchange as the dominant mechanism, with calculated energy values (E) between 8.64–9.13 kJ/mol. The intraparticle diffusion model further elucidated the rate-limiting steps, identifying boundary layer diffusion as a significant factor, especially in the case of Tuzla water. The results also underscore the importance of optimizing adsorbent dosage to balance recovery efficiency and operational feasibility, with recovery efficiencies reaching 95% for Germencik and 80% for Tuzla under optimal conditions. An effective chromatographic separation of Li using CTS/HMO adsorbent was achieved with a total adsorption capacity of 0.63 mg Li/mL adsorbent and a column utilization efficiency of 69.03% for a model Li solution. The desorption process was highly efficient, with a peak Li concentration of 43 mg/L at 9 BV and an elution efficiency of 76%. This work developed the potential of CTS/HMO composites as efficient, eco-friendly solutions for Li recovery, paving the way for their application in industrial-scale operations. Future research focusing on regenerability, economic feasibility, and the environmental impact of this adsorbent can further enhance its practical utility, especially in the context of rising Li demands driven by the global transition to renewable energy and electric vehicles.

## Acknowledgment

This study was financially supported by the Research Universities Support Program of the Higher Education Council of Türkiye (Grant No: 2022IYTE-2-0009). We acknowledge "The Environmental Research and Development Center" for ICP-OES analyses at the Izmir Institute of Technology Integrated Research Center.

## References

[1] N. Bolan, S.A. Hoang, M. Tanveer, L. Wang, S. Bolan, P. Sooriyakumar, B. Robinson, H. Wijesekara, M. Wijesooriya, S. Keerthanan, From mine to mind and mobiles–Lithium contamination and its risk management, Environ Pollut, 290 (2021) 118067.

[2] D. Chandrasekharam, M.F. Şener, Y.K. Recepoğlu, T. Isık, M.M. Demir, A. Baba, Lithium: An energy transition element, its role in the future energy demand and carbon emissions mitigation strategy, Geothermics 119 (2024) 102959.

[3] G. Calvo, A. Valero, A. Valero, Assessing maximum production peak and resource availability of non-fuel mineral resources: Analyzing the influence of extractable global resources, Resour Conserv Recycl 125 (2017) 208–217.

[4] Y.K. Recepoğlu, Optimized Lithium (I) Recovery from Geothermal Brine of Germencik, Türkiye, Utilizing an Aminomethyl phosphonic Acid Chelating Resin, Solvent Extr Ion Exch, (2024) 1–22.

[5] P. Christmann, E. Gloaguen, J.-F. Labbé, J. Melleton, P. Piantone, Global lithium resources and sustainability issues, in: Lithium Process Chemistry, Elsevier, 2015: pp. 1–40.

[6] R. Millot, A. Hegan, P. Négrel, Geothermal waters from the Taupo volcanic zone, New Zealand: Li, B and Sr isotopes characterization, Appl Geochem, 27 (2012) 677–688.

[7] Z. Qin, L. He, J. Duo, M. Li, Y. Li, Q. Du, G. Zhang, G. Wu, G. Liu, Origin and evolution of Li-rich geothermal waters from the

Kawu geothermal system, Himalayas: based on hydrochemistry and HO, Li isotopes, Int Geol Rev 66 (2024) 1519–1534.

[8] B. Sanjuan, B. Gourcerol, R. Millot, D. Rettenmaier, E. Jeandel, A. Rombaut, Lithium-rich geothermal brines in Europe: An up-date about geochemical characteristics and implications for potential Li resources, Geothermics 101 (2022) 102385.

[9] J. Li, X. Wang, C. Ruan, G. Sagoe, J. Li, Enrichment mechanisms of lithium for the geothermal springs in the southern Tibet, China, J Hydrol (Amst) 612 (2022) 128022.

[10] A. Gökgöz, G. Tarcan, Mineral equilibria and geothermometry of the Dalaman–Köyceğiz thermal springs, southern Turkey, Appl Geochem, 21 (2006) 253–268.

[11] A. Vengosh, C. Helvacı, İ.H. Karamanderesi, Geochemical constraints for the origin of thermal waters from western Turkey, Appl Geochem, 17 (2002) 163–183.

[12] S. Pasvanoğlu, Geochemistry and conceptual model of thermal waters from Erciş-Zilan Valley, Eastern Turkey, Geothermics 86 (2020) 101803.

[13] E.H. Temizel, F. Gültekin, A.F. Ersoy, R.K. Gülbay, Multi-isotopic (O, H, C, S, Sr, B, Li) characterization of waters in a low-enthalpy geothermal system in Havza (Samsun), Turkey, Geothermics 97 (2021) 102240.

[14] S. S. Rangarajan, S.P. Sunddararaj, A.V. V Sudhakar, C.K. Shiva, U. Subramaniam, E.R. Collins, T. Senjyu, Lithium-ion batteries—The crux of electric vehicles with opportunities and challenges, Clean Technol, 4 (2022) 908–930.

[15] Y. Miao, P. Hynan, A. Von Jouanne, A. Yokochi, Current Li-ion battery technologies in electric vehicles and opportunities for advancements, Energies (Basel) 12 (2019) 1074.

[16] Y. Ding, Z.P. Cano, A. Yu, J. Lu, Z. Chen, Automotive Li-ion batteries: current status and future perspectives, Electrochem Energy Rev, 2 (2019) 1–28.

[17] A. Khalil, S. Mohammed, R. Hashaikeh, N. Hilal, Lithium recovery from brine: Recent developments and challenges, Desalination 528 (2022) 115611.

[18] S. Sahu, A. Mohanty, N. Devi, Application of various extractants for liquid-liquid extraction of lithium, Mater Today Proc 76 (2023) 190–193.

[19] J. Zhu, A. Asadi, D. Kang, J.C.-Y. Jung, P.-Y.A. Chuang, P.-C. Sui, Bipolar membranes electrodialysis of lithium sulfate solutions from hydrometallurgical recycling of spent lithium-ion batteries, Sep Purif Technol 354 (2025) 128715.

[20] X. Chen, X. Ruan, S.E. Kentish, G.K. Li, T. Xu, G.Q. Chen, Production of lithium hydroxide by electrodialysis with bipolar membranes, Sep Purif Technol 274 (2021) 119026.

[21] B. Swain, Separation and purification of lithium by solvent extraction and supported liquid membrane, analysis of their mechanism: a review, J Chem Technol Biotechnol, 91 (2016) 2549–2562.

[22] M.R. Mojid, K.J. Lee, J. You, A review on advances in direct lithium extraction from continental brines: Ion-sieve adsorption and electrochemical methods for varied Mg/Li ratios, Sustain Mater Technol, (2024) e00923.

[23] S. Ye, C. Yang, Y. Sun, C. Guo, J. Wang, Y. Chen, C. Zhong, T. Qiu, Application and Mechanism of Lithium-ion Sieves in the Recovery of Lithium-Containing Wastewater: a Review, Water Air Soil Pollut 235 (2024) 272.

[24] S. Chen, Z. Chen, Z. Wei, J. Hu, Y. Guo, T. Deng, Titanium-based ion sieve with enhanced post-separation ability for high performance lithium recovery from geothermal water, Chem Eng J, 410 (2021) 128320.

[25] X. Xu, Y. Chen, P. Wan, K. Gasem, K. Wang, T. He, H. Adidharma, M. Fan, Extraction of lithium with functionalized lithium ion-sieves, Prog Mater Sci 84 (2016) 276–313.

[26] Y. Orooji, Z. Nezafat, M. Nasrollahzadeh, N. Shafiei, M. Afsari, K. Pakzad, A. Razmjou, Recent advances in nanomaterial development for lithium ion-sieving technologies, Desalination 529 (2022) 115624.

[27] J. Xiao, X. Nie, S. Sun, X. Song, P. Li, J. Yu, Lithium ion adsorption–desorption properties on spinel $Li_4Mn_5O_{12}$ and pH-dependent ion-exchange model, Adv Powder Technol, 26 (2015) 589–594.

[28] J.-L. Xiao, S.-Y. Sun, J. Wang, P. Li, J.-G. Yu, Synthesis and adsorption properties of Li1. 6Mn1. 6O4 spinel, Ind Eng Chem Res 52 (2013) 11967–11973.

[29] Q.-H. Zhang, S. Sun, S. Li, H. Jiang, J.-G. Yu, Adsorption of lithium ions on novel nanocrystal MnO2, Chem Eng Sci 62 (2007) 4869–4874.

[30] Y.K. Recepoğlu, N. Kabay, İ. Yılmaz-Ipek, M. Arda, K. Yoshizuka, S. Nishihama, M. Yüksel, Equilibrium and Kinetic Studies on Lithium Adsorption from Geothermal Water by λ-MnO2, Solvent Extr Ion Exch, 35 (2017) 221–231.

[31] Y.K. Recepoğlu, N. Kabay, K. Yoshizuka, S. Nishihama, İ. Yılmaz-Ipek, M. Arda, M. Yüksel, Effect of Operational Conditions on Separation of Lithium from Geothermal Water by λ-MnO2 Using Ion Exchange–Membrane Filtration Hybrid Process, Solvent Extr Ion Exch, 36 (2018) 499–512.

[32] Y.K. Recepoğlu, N. Kabay, İ. Yılmaz-Ipek, M. Arda, M. Yüksel, K. Yoshizuka, S. Nishihama, Elimination of boron and lithium coexisting in geothermal water by adsorption-membrane filtration hybrid process, Sep Sci Technol, (Philadelphia) 53 (2018) 856–862.

[33] G.M. Nisola, L.A. Limjuco, E.L. Vivas, C.P. Lawagon, M.J. Park, H.K. Shon, N. Mittal, I.W. Nah, H. Kim, W.-J. Chung, Macroporous flexible polyvinyl alcohol lithium adsorbent foam composite prepared via surfactant blending and cryo-desiccation, Chem Eng J, 280 (2015) 536–548.

[34] S. Wei, Y. Wei, T. Chen, C. Liu, Y. Tang, Porous lithium ion sieves nanofibers: General synthesis strategy and highly selective recovery of lithium from brine water, Chem Eng J, 379 (2020) 122407.

[35] G. Zhang, C. Hai, Y. Zhou, J. Zhang, Y. Liu, J. Zeng, Y. Shen, X. Li, Y. Sun, Z. Wu, Synthesis and performance estimation of a granulated PVC/PAN-lithium ion-sieve for Li+ recovery from brine, Sep Purif Technol 305 (2023) 122431.

[36] J.-L. Xiao, S.-Y. Sun, X. Song, P. Li, J.-G. Yu, Lithium ion recovery from brine using granulated polyacrylamide–MnO2 ion-sieve, Chem Eng J, 279 (2015) 659–666.

[37] I.A. Udoetok, A.H. Karoyo, E.E. Ubuo, E.D. Asuquo, Granulation of Lithium-Ion Sieves Using Biopolymers: A Review, Polymers (Basel) 16 (2024) 1520.

[38] Y.K. Recepoğlu, B. Arabacı, A. Kahvecioğlu, A. Yüksel, Granulation of hydrometallurgically synthesized spinel lithium manganese oxide using cross-linked chitosan for lithium adsorption from water, J Chromatogr A (2024) 464712.

[39] I. Langmuir, The constitution and fundamental properties of solids and liquids. Part II.-Liquids, J Franklin Inst 184 (1917) 721.

[40] I. Langmuir, The constitution and fundamental properties of solids and liquids. Part I. Solids., J Am Chem Soc 38 (1916) 2221–2295.

[41] H. Freundlich, Über die adsorption in lösungen, Z Phys Chem, 57 (1907) 385–470.

[42] C. Nguyen, D.D. Do, The Dubinin–Radushkevich equation and the underlying microscopic adsorption description, Carbon, 39 (2001) 1327–1336.

[43] E.D. Revellame, D.L. Fortela, W. Sharp, R. Hernandez, M.E. Zappi, Adsorption kinetic modeling using pseudo-first order and pseudo-second order rate laws: A review, Clean Eng Technol 1 (2020) 100032.

[44] Y.-S. Ho, Review of second-order models for adsorption systems, J Hazard Mater 136 (2006) 681–689.

[45] Y.-S. Ho, Second-order kinetic model for the sorption of cadmium onto tree fern: a comparison of linear and non-linear methods, Water Res 40 (2006) 119–125.

[46] W.J. Weber, J.C. Morris, Kinetics of adsorption on carbon from solution, J Sanit Eng Div ASCE, 89 (1963) 31–60.

[47] Y.K. Recepoğlu, A. Yüksel, Cross-Linked Phosphorylated Cellulose as a Potential Sorbent for Lithium Extraction from Water: Dynamic Column Studies and Modeling, ACS Omega 7 (2022) 38957–38968.

[48] H. Jiang, Y. Yang, J. Yu, Application of concentration-dependent HSDM to the lithium adsorption from brine in fixed bed columns, Sep Purif Technol 241 (2020) 116682.

[49] C. Geankoplis, Transport processes and separation process principles (includes unit operations), Prentice Hall Press, 2003.

[50] B. Sever, E. Altıok, Y. Abdullahi Jarma, K. Bostancı, N. Kabay, M. Arda, S. Nishihama, K. Yoshizuka, Lithium Recovery from Reverse Osmosis Concentrate of Geothermal Water by Spinel Type λ-MnO2-Batch Tests, Solvent Extr Ion Exch (2025) 1–20.

[51] H. Patel, Fixed-bed column adsorption study: a comprehensive review, Appl Water Sci 9 (2019) 45.

[52] S. Toprak, Ç. Öncel, S. Yılmaz, A. Baba, G.A. Koç, M.M. Demir, Lithium extraction from geothermal brine using γ-MnO2: A case study for Tuzla geothermal power plant, Heliyon 10 (2024).

[53] R. Chitrakar, H. Kanoh, Y. Miyai, K. Ooi, Recovery of lithium from seawater using manganese oxide adsorbent (H1.6Mn1.6O4) derived from Li1.6Mn1.6O4, Ind Eng Chem Res 40 (2001) 2054–2058.

[54] K.S. Chung, M.A. Kim, H. Lee, Y.J. Suh, D.S. Kil, B.C. Dave, J.C. Lee, Preparation of ion-sieve type (H)[M0. 5Mn1. 5] O4 (M= Mg, Zn) and their lithium adsorption properties in seawater, Solid State Phenom 124 (2007) 739–742.

[55] S.-Y. Sun, J.-L. Xiao, J. Wang, X. Song, J.-G. Yu, Synthesis and adsorption properties of Li1. 6Mn1. 6O4 by a combination of redox precipitation and solid-phase reaction, Ind Eng Chem Res 53 (2014) 15517–15521.

[56] G. Cao, X. Yang, Z. Yin, Y. Lei, H. Wang, J. Li, Synthesis, adsorption properties and stability of Cr-doped lithium ion sieve in salt lake brine, Bull Chem Soc Jpn 92 (2019) 1205–1210.